



Surface-Plasmon Holography with White-Light Illumination

Miyu Ozaki, et al. Science **332**, 218 (2011); DOI: 10.1126/science.1201045

This copy is for your personal, non-commercial use only.

If you wish to distribute this article to others, you can order high-quality copies for your colleagues, clients, or customers by clicking here.

Permission to republish or repurpose articles or portions of articles can be obtained by following the guidelines here.

The following resources related to this article are available online at www.sciencemag.org (this infomation is current as of May 4, 2011):

Updated information and services, including high-resolution figures, can be found in the online version of this article at:

http://www.sciencemag.org/content/332/6026/218.full.html

Supporting Online Material can be found at:

http://www.sciencemag.org/content/suppl/2011/04/06/332.6026.218.DC1.html

This article **cites 18 articles**, 1 of which can be accessed free: http://www.sciencemag.org/content/332/6026/218.full.html#ref-list-1

This article appears in the following **subject collections**: Physics

http://www.sciencemag.org/cgi/collection/physics

We have constrained the parameters of the BC pair by modeling the short-period eclipses in the Kepler band using the jktebop code (16, 17). The ratio of the radii of the B and C components is poorly constrained at present, partly because of the low sampling rate of the Kepler LC data. The A component contributes 99.29% of the system light in the Kepler passband, and the BC pair contribute 0.44% and 0.27%, respectively. Taking the V-band absolute magnitude of HD 181068 A to be $M_V(A) = -0.3$ and assuming that our results for the Kepler passband are representative of the V band, we find $M_V(B) = 5.6$ and $M_V(C) = 6.1$. Such absolute magnitudes indicate spectral types of G8 V and K1 V for stars B and C, respectively (18). Because we do not have independent measurements of $T_{\rm eff}$ for the BC pair, we can only estimate their masses based on their spectral types. This indicates that their masses are about $0.7 \pm$ $0.1 M_{\odot}$ each (6).

One puzzling feature of the system is the short-period fluctuations that have the largest amplitudes when the BC pair is behind star A, while remaining apparent with a slowly changing amplitude in all the other phases of the wide orbit. We have investigated this variability of HD 181068 A with a detailed frequency analysis and a comparison to other red giant stars that have similar properties (6). The frequency content of the light curve suggests an intimate link to tidal effects in the triple system, with the first four dominant peaks in the power spectrum identifiable as simple linear combinations of the two orbital frequencies. On the other hand, solarlike oscillations (meaning those excited by nearsurface convection, as in the Sun but also observed in red giants) that are expected to produce an equidistant series of peaks in the power spectrum are not visible, even though all stars with similar parameters in the Kepler database do show clear evidence of these oscillations. In other words, the convectively driven solarlike oscillations that we would expect to see in a giant of this type seem to have been suppressed (6).

In a recent compilation of 724 triple stars (19), there is only one system with an outer orbital period shorter than that of HD 181068 (λ Tau, for which $P_{\text{out}} = 33.03$ days). Carter *et al.* (20) reported the discovery of KOI-126 with a similarly short outer period ($P_{\text{out}} = 33.92 \text{ days}$). Extremely compact hierarchical triple systems form a very small minority of hierarchical triplets, with only 7 of the catalogized 724 systems having outer periods shorter than 150 days. Furthermore, HD 181068 and KOI-126 have the highest outer mass ratios [~ 2.1 and 3, defined as $m_A/(m_B +$ $m_{\rm C}$)] among the known systems. In 97% of the known hierarchical triplets before the Kepler era, the mass of the close binary exceeded that of the wider companion, and even the largest outer mass ratio remained under 1.5. It is not yet clear whether this rarity of such systems is caused by an observational selection effect or has an underlying stellar evolutionary or dynamical explanation.

Its properties make HD 181068 an ideal target for dynamical evolutionary studies and for testing tidal friction theories. Because of its compactness and its massive primary, we can expect short-term orbital element variations on two different time scales of 46 days (i.e., with period of $P_{\text{A-BC}}$) and about 6 years ($P_{\text{A-BC}}^2/P_{\text{BC}}$), the time scale of the classical apsidal motion and nodal regression (21), which for the triply eclipsing nature could be observed relatively easily.

References and Notes

- 1. W. J. Borucki et al., Science 327, 977 (2010).
- 2. D. G. Koch *et al.*, *Astrophys. J.* **713**, L79 (2010).
- 3. J. M. Jenkins et al., Astrophys. J. 713, L87 (2010).
- J. M. Jenkins et al., Astrophys. J. 713, L120 (2010).
 P. Guillout et al., Astron. Astrophys. 504, 829 (2009).
- 6. Materials and methods are available as supporting
- 6. Materials and methods are available as supporting material on *Science* Online.
- 7. Available at http://archive.stsci.edu/kepler/.
- M. J. Ireland et al., in Optical and Infrared Interferometry, M. Scholler, W. C. Danchi, F. Delplancke, Eds., vol. 7013 of Proceedings of the SPIE (Society of Photo-Optical Instrumentation Engineers, Bellingham, WA, 2008), pp. 701324–701324-10.
- 9. T. A. ten Brummelaar et al., Astrophys. J. 628, 453 (2005).

- R. Hanbury Brown et al., Mon. Not. R. Astron. Soc. 167, 475 (1974).
- F. van Leeuwen, Hipparcos, the New Reduction of the Raw Data (Astrophysics and Space Science Library, Springer, Berlin, 2007), vol. 350.
- 12. O. C. Wilson, M. K. V. Bappu, Astrophys. J. 125, 661 (1957).
- G. Pace, L. Pasquini, S. Ortolani, Astron. Astrophys. 401, 997 (2003).
- 14. A. Pietrinferni, S. Cassisi, M. Salaris, F. Castelli, *Astrophys. J.* **612**, 168 (2004).
- 15. L. Girardi, Mon. Not. R. Astron. Soc. 308, 818 (1999).
- J. Southworth, S. Zucker, P. F. L. Maxted, B. Smalley, Mon. Not. R. Astron. Soc. 355, 986 (2004).
- J. Southworth, B. Smalley, P. F. L. Maxted, A. Claret,
 P. B. Etzel, Mon. Not. R. Astron. Soc. 363, 529 (2005).
- 18. A. N. Cox, *Allen's Astrophysical Quantities* (Springer, New York, 2000).
- 19. A. A. Tokovinin, Mon. Not. R. Astron. Soc. 389, 925 (2008).
- 20. J. A. Carter *et al.*, *Science* **331**, 562 (2011); 10.1126/science.1201274.
- 21. E. W. Brown, Mon. Not. R. Astron. Soc. 97, 62 (1936).
- 22. A.D. is a Magyary Zoltán Postdoctoral Research Fellow. Funding for this Discovery mission is provided by NASA's Science Mission Directorate. The authors gratefully acknowledge the entire Kepler team, whose outstanding efforts have made these results possible. This project has been supported by Hungarian Scientific Research Fund (OTKA) grants K76816, K83790, and MB08C 81013; the "Lendület" Program of the Hungarian Academy of Sciences: and the Magyary Zoltán Higher Educational Public Foundation. The DAO observations were supported by an American Astronomical Society Small Research Grant. The CHARA Array is owned by Georgia State University. Additional funding for the CHARA Array is provided by NSF under grant AST09-08253, the W. M. Keck Foundation, and the NASA Exoplanet Science Center. TLS observations were done as a part of the Deutsche Forschungsgemeinschaft grant HA 3279/5-1. For her research, C.A. received funding from the European Research Council (ERC) under the European Community's Seventh Framework Programme (FP7/2007-2013)/ERC grant agreement no. 227224 (Prosperity).

Supporting Online Material

www.sciencemag.org/cgi/content/full/332/6026/216/DC1 Materials and Methods Figs. S1 to S3 Tables S1 to S3 References SOM Data

15 December 2010; accepted 3 March 2011 10.1126/science.1201762

Surface-Plasmon Holography with White-Light Illumination

Miyu Ozaki, 1,2 Jun-ichi Kato, 1 Satoshi Kawata 1,3*

The recently emerging three-dimensional (3D) displays in the electronic shops imitate depth illusion by overlapping two parallax 2D images through either polarized glasses that viewers are required to wear or lenticular lenses fixed directly on the display. Holography, on the other hand, provides real 3D imaging, although usually limiting colors to monochrome. The so-called rainbow holograms—mounted, for example, on credit cards—are also produced from parallax images that change color with viewing angle. We report on a holographic technique based on surface plasmons that can reconstruct true 3D color images, where the colors are reconstructed by satisfying resonance conditions of surface plasmon polaritons for individual wavelengths. Such real 3D color images can be viewed from any angle, just like the original object.

oble metal films, such as silver and gold foil, contain free electrons that collectively oscillate and propagate as the surface

wave in optical frequency region. The quantum of this surface wave is called surface plasmon polariton (SPP) (1). The electromagnetic field gen-

erated by SPP can be enhanced and strongly confined spatially in the near field (with the distance less than the wavelength) from the metal surface as a nonirradiative evanescent field (2, 3). The ability to confine and enhance the optical field to the vicinity of the metal surface or nanometal particle has been applied to immuno-sensor (4), fluorescence sensor (5), solar cell (6), plasmonic laser (7, 8), nanomicroscopy (9, 10), super-lens (11, 12) and photodynamic cancer cell treatment (13).

We report an application of SPP to threedimensional (3D) color holography with white-

¹RIKEN, Wako, Saitama 351-0198, Japan. ²Department of Robotics and Mechatronics, Tokyo Denki University, Chiyoda-ku, Tokyo 101-8457, Japan. ³Department of Applied Physics and Photonics Advanced Research Center, Osaka University, Suita, Osaka, 565-0871, Japan.

*To whom correspondence should be addressed. E-mail: kawata@skawata.com

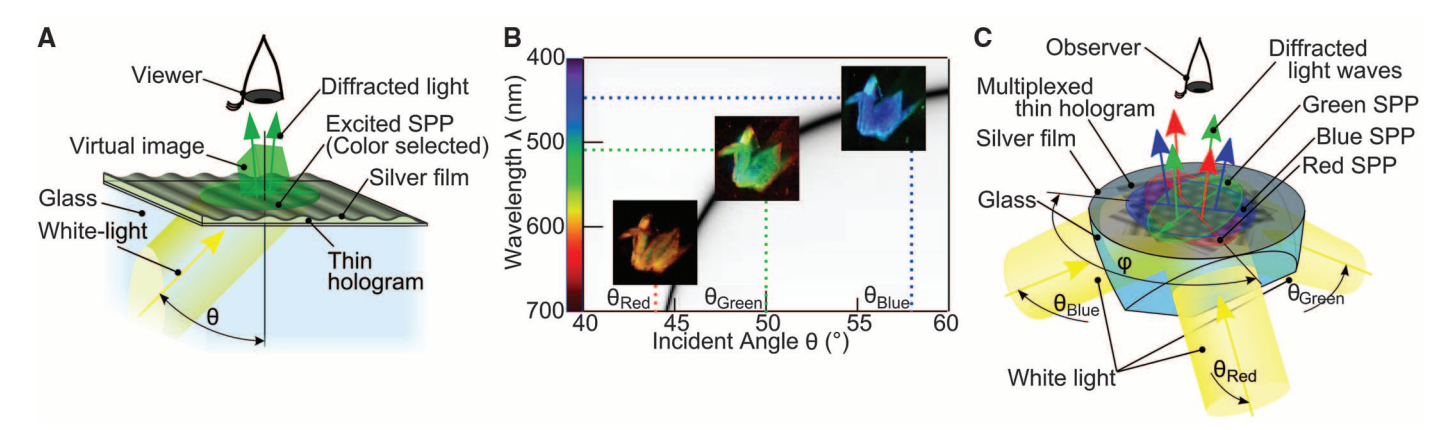


Fig. 1. Surface plasmon hologram and its color reconstruction with white-light illumination. **(A)** The SPP hologram is illuminated by white light at a given angle θ in high-index medium. Surface plasmons of a selected color are excited and diffracted by the SPP hologram to reconstruct the wavefront of the object. **(B)** Dispersion curve of the SPP hologram in reconstruction as a function of the incident

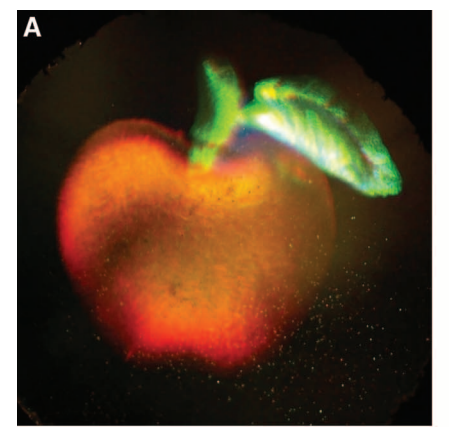
angle of white light. The 3D images of red, green, and blue cranes made of paper are obtained at different angles with white-light illumination. This curve was obtained through calculations based on Fresnel's equations. (C) Reconstruction of a color object through SPP hologram. The hologram is illuminated simultaneously with a white light in three directions at different angles θ and ϕ for each.

light illumination. The first idea to use plasmons for holography was published as a reflection type by Cowan (14), and since then authors have reported holographic reconstruction of transmission type (15–17). In those configurations, plasmons have been used for enhancing the diffraction efficiency. In this report, we use color selectivity of SPPs for holographic color reconstruction with white-light illumination.

We recorded the hologram on a photoresist as an interference pattern between a light field coming from the object as scattered light and the unscattered reference beam. Exposure was repeated three times with rotation of the illumination angle for a single color hologram recording. Instead of rotation, one can also use three lasers simultaneously to obtain the hologram in a single exposure. A thin metal film is then coated on the photoresist hologram, which is precoated on a glass plate. For image reconstruction, the SPP is excited by a color component of white light that is incident on the metal film through a prism with an angle satisfying the condition of total internal reflection (Fig. 1A). The SPP associates with a nonradiative evanescent light wave on metal film and then is converted by the grating component of hologram into a radiative light field, which represents the reconstructed wavefront of light that scattered at the object. The reconstruction of the prerecorded object is seen with the eyes through an SPP hologram in color. The reference beam or the zeroth-order diffraction as background beam does not exist in reconstruction for this configuration because the illumination of the hologram is made by total internal reflection.

Figure 1B shows the dispersion curve of SPP with wavelength λ as a function of the incident angle θ of illumination (excitation). This relationship is given as

$$\theta = \sin^{-1} \left(\frac{1}{n_{\text{glass}}} \sqrt{\frac{n_m^2 n(\lambda)^2}{n_m^2 + n(\lambda)^2}} \right)$$
 (1)



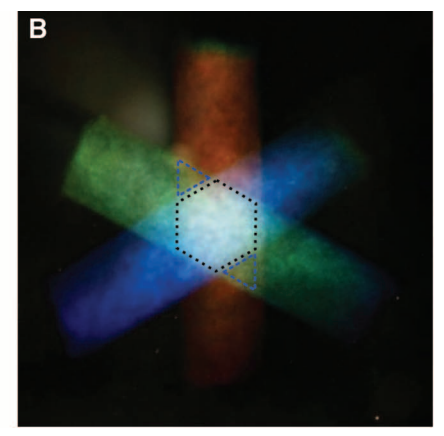


Fig. 2. Reconstruction of three-dimensional color objects through surface plasmon holograms. (**A**) Red apple with green leaf in three dimensions (see movie S1). (**B**) Color bar recorded three times with red, green, and blue by rotating the bar by 120° for each color. In the center, where the three colors overlap, a hexagonal area is reconstructed as white, whereas yellow triangles are reconstructed where red and green overlap.

where $n_{\rm glass}$, n_m , and $n(\lambda)$ are the refractive index of the glass substrate, effective index of the medium on the metal surface, and the index of metal (which is a function of λ), respectively (2).

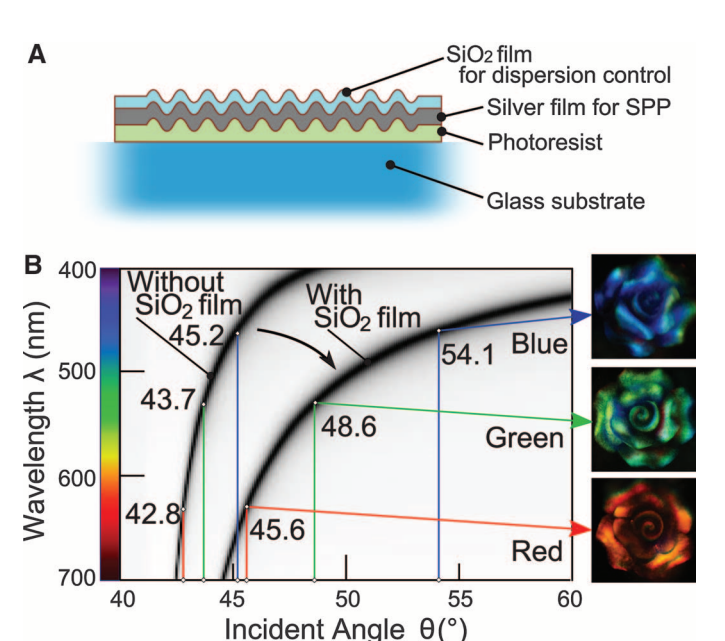
Individual colors are reconstructed by illumination at corresponding incident angles by satisfying the above relationship for each color. Figure 1C shows the optical setup for reconstructing a three-color object in different azimuthal and incident angle sets $[(\phi_R, \theta_R), (\phi_G, \theta_G),$ and $(\phi_B, \theta_B)]$ with white-light illumination.

Reconstruction of an object, an apple with a leaf, is seen in 3D from the thin film plasmon hologram (Fig. 2A) (18). A movie of the object taken with a camera moving around the object is provided (movie S1) in the supporting online material. For plasmon color holography, the adjustment of the white color balance is important for representing the natural color of an object or a scene. We obtained the white color balance by carefully controlling the power of the laser with

multiple exposures for red (R), green (G), and blue (B). Figure 2B shows an image of a bar taken by three-time exposure in R, G, and B; each exposure was made by rotating the object (bar) and by taking shots at every 120° of rotation. It includes a white hexagon in the center where all three colors overlap and yellow triangles where red and green bars overlap. For reconstruction of the object, a 100-W Halogen lamp is used.

Figure 3A shows the multilayer system of an SPP hologram. The role of the top-layer dielectric film is to enhance the spectral separation in reconstruction. If this film is absent, the angular separation for the three colors R, G, and B in reconstruction is not large enough (less than 3° between red and blue; more precisely, the angles for the three colors are at 42.8°, 43.7°, and 45.2°, respectively) in a dispersion relationship (Fig. 3B) and makes it difficult to practically reconstruct a color object. If the SiO₂ film is coated, the angular separation between red and blue be-

Fig. 3. Multilayer system and the color dispersion of an SPP hologram. (A) Hologram configuration. From the top, dielectric layer (25-nm-thick SiO₂), metal layer (55nm-thick silver), and dielectric substrate with 25-nm depth modulation (150-nm-thick photoresist on the glass). (B) The top SiO₂ layer works for expanding the color dispersion to incident angle. Without the SiO₂ layer on the hologram, the angular separation for color reconstruction is small. Rose pendants of red, green, and blue are separated in the reconstruction, as shown in the insets.



comes as large as 10° due to the higher index $n_{\rm m}$ of film; more precisely, the angles for the three colors are at 45.6° , 48.6° , and 54.1° , respectively. In Fig. 3B, theoretical curves are plotted from the calculation of a multilayer system based on Fresnel's equations for noncoated and coated SPP holograms. A rose pendant in the figure is decomposed into three colors in reconstruction by choosing the angle for white-light illumination (Fig. 3B).

Our results show that plasmon color holography provides a view of an object or a scene seen naturally and vitally with white-light illumination. A typical amplitude modulation in plasmon hologram is ~25 nm (fig. S2), which is much

thinner compared with Lippmann-Denisyuk's color hologram (19) based on Bragg diffraction in volume. The rainbow holograms mounted, for example, on credit cards (20) also reconstruct with white light, where color varies with viewing angle but not with the color distribution in the object. Plasmon holography is advantageous in terms of background-beam—free reconstruction because the illumination light is totally reflected back at the hologram (21). Plasmon holography does not suffer from the ghost produced by the diffraction of ambient light or higher orders of diffraction, because those components are not coupled with SPPs.

References and Notes

- 1. l. Heber, Nature 461, 720 (2009).
- 2. H. Raether, Surface Plasmons on Smooth and Rough surfaces and on Gratings (Springer, Berlin, 1988).
- 3. S. Kawata, *Near Field Optics and Surface Plasmon Polaritons* (Springer, Berlin, 2001).
- B. Liedberg, C. Nylander, I. Lunström, Sens. Actuators 4, 299 (1983).
- 5. H. Kano, S. Kawata, Opt. Lett. 21, 1848 (1996).
- V. E. Ferry, L. A. Sweatlock, D. Pacifici, H. A. Atwater, Nano Lett. 8, 4391 (2008).
- T. Okamoto, F. H'Dhili, S. Kawata, Appl. Phys. Lett. 85, 3968 (2004).
- 8. N. I. Zheludev, S. L. Prosvirnin, N. Papasimakis, V. A. Fedotov, *Nat. Photonics* **2**, 351 (2008).
- 9. S. Kawata, Y. Inouye, P. Verma, *Nat. Photonics* **3**, 388 (2009).
- N. Hayazawa, Y. Inouye, Z. Sekkat, S. Kawata, Opt. Commun. 183, 333 (2000).
- 11. J. B. Pendry, Phys. Rev. Lett. 85, 3966 (2000).
- 12. N. Fang, H. Lee, C. Sun, X. Zhang, Science 308, 534 (2005).
- C. Loo, A. Lowery, N. Halas, J. West, R. Drezek, *Nano Lett.* 5, 709 (2005).
- 14. J. J. Cowan, Opt. Commun. 5, 69 (1972).
- S. Maruo, O. Nakamura, S. Kawata, Appl. Opt. 36, 2343 (1997)
- G. P. Wang, T. Sugiura, S. Kawata, Appl. Opt. 40, 3649 (2001).
- M. Ozaki, J. Kato, R. Furutani, S. Kawata, J. Jpn. Soc. Precision Eng. 74, 1113 (2008).
- Materials and methods are available as supporting materials on Science Online.
- 19. Yu. N. Denisyuk, Sov. Phys. Dokl. 7, 543 (1962).
- 20. S. A. Benton, J. Opt. Soc. Am. 59, 1545 (1969).
- 21. O. Bryngdahl, J. Opt. Soc. Am. 59, 1645 (1969).
- 22. S. Kawata conceived the research and planned the experiments. M. Ozaki conducted the experiment and calculations. All authors discussed the results and contributed in preparing the manuscript. The authors thank R. Furutani for discussion and P. Verma for his review.

Supporting Online Material

www.sciencemag.org/cgi/content/full/332/6026/218/DC1 Materials and Methods Figs. S1 and S2

References Movie S1

30 November 2010; accepted 24 February 2011 10.1126/science.1201045

The Hot Summer of 2010: Redrawing the Temperature Record Map of Europe

David Barriopedro, ¹* Erich M. Fischer, ² Jürg Luterbacher, ³ Ricardo M. Trigo, ¹ Ricardo García-Herrera ⁴

The summer of 2010 was exceptionally warm in eastern Europe and large parts of Russia. We provide evidence that the anomalous 2010 warmth that caused adverse impacts exceeded the amplitude and spatial extent of the previous hottest summer of 2003. "Mega-heatwaves" such as the 2003 and 2010 events likely broke the 500-year-long seasonal temperature records over approximately 50% of Europe. According to regional multi-model experiments, the probability of a summer experiencing mega-heatwaves will increase by a factor of 5 to 10 within the next 40 years. However, the magnitude of the 2010 event was so extreme that despite this increase, the likelihood of an analog over the same region remains fairly low until the second half of the 21st century.

Increasing greenhouse gas concentrations are expected to amplify the variability of summer temperatures in Europe (*1*–5). Along with mean warming, enhanced variability results in more frequent, persistent, and intense heatwaves

(6-10). Consistent with these expectations, Europe has experienced devastating heatwaves in recent years. The exceptional summer of 2003 (1, 11-13) caused around 70,000 heat-related deaths, mainly in western and central Europe

(14). In summer 2010, many cities in eastern Europe recorded extremely high values of daytime (for example, Moscow reached 38.2°C), night-time (Kiev reached 25°C), and daily mean (Helsinki reached 26.1°C) temperatures (fig. S1). Preliminary estimates for Russia referred a death toll of 55,000, an annual crop failure of ~25%, more than 1 million ha of burned areas, and ~US\$15 billion (~1% gross domestic product) of total economic loss (15). During the same period, parts of eastern Asia also experienced extremely warm temperatures, and Pakistan was hit by devastating monsoon floods.

In order to characterize the magnitude and spatio-temporal evolution of the 2010 event in a historical context, we used daily mean data sets

¹Instituto Dom Luiz, University of Lisbon, 1749-016 Lisbon, Portugal. ²Institute for Atmospheric and Climate Science, Eidgenössische Technische Hochschule (ETH) Zurich, 8092 Zurich, Switzerland. ³Department of Geography, Justus-Liebig-University of Giessen, D-35390 Giessen, Germany. ⁴Agencia Estatal de Meteorología (AEMET), 28071 Madrid, Spain.

^{*}To whom correspondence should be addressed. E-mail: dbarriopedro@fc.ul.pt